Gas Dispersion in Air-Lift Reactors: Contribution of the Turbulent Part of the Added Mass Force

Rahmani Mohamed Ali, Chahed Jamel and Bellakhal Ghazi
LMHE, Ecole Nationale des Ingénieurs de Tunis, BP N○37, Le Belvédère, 1002 Tunis, Tunisie

Alain Line
L1SBP, UMR INSA-CNRS 5504 and INSA-INRA 792, 135 avenue de Rangueil, 31077 Toulouse, France

DOI 10.1002/aic.12539
Published online April 28, 2011 in Wiley Online Library (wileyonlinelibrary.com).

Gas dispersion in an airlift reactor focusing on the closure law on turbulent contribution of added mass is presented. A data bank for bubbly flow in an airlift reactor is presented. The liquid velocity is measured by hot film anemometry and gas fraction and velocity are measured with an optical probe. The sensitivity of numerical simulations of gas dispersion to the modeling of turbulent contribution of added mass is shown. Without the turbulent contribution, the bubbles move toward the region where the turbulence is high and the pressure is low. When the turbulent contribution is introduced, the bubble migration towards the low pressure region is counter-balanced and the void fraction profile is significantly modified. The modeling of the turbulent contribution of added mass is expressed in terms of the turbulent correlations in the gas phase, $\overline{u'_{Gi}u'_{Gj}}$, that can be related to the Reynolds stress in the liquid phase, $\overline{u'_i u'_j}$.
 AIChE J, 57: 3315–3330, 2011
Keywords: airlift, hydrodynamics, two-fluid model, turbulence, computational fluid dynamics

Introduction

Gas–liquid reactors are used industrially, for instance, in the field of chemical engineering, biotechnology, and water treatment. In particular, bubble columns and airlift reactors have three main advantages: the first is their low-energy consumption; the second is the large interfacial area; and the third is the presence of low-shear stresses, avoiding cell damage in bioreactor application. Thus, scaling of mixing and mass transfer in bubble columns and airlift reactors is of significant industrial importance. However, scaling-up bubble columns and airlift reactors remains difficult. Part of the difficulty lies in the fact that in large scale reactors, the spatial heterogeneity of bubble distribution within the reactor, in terms of phase fraction and bubble size, is increased, in comparison with the pilot scale. Indeed, the spatial heterogeneity of bubble distribution within the reactor is mainly due to gas dispersion. Therefore, this article addresses gas dispersion in air lift reactor.

The analysis of the experiments in bubbly flows indicates that in comparison with single phase flows, the structure of the turbulence can be modified in various ways. In two-phase bubbly flows with low turbulence intensities (for example, weakly shear flows), the presence of bubbles confers a significant increase of the turbulence by comparison with the equivalent single phase case.[1,2] The experimental results of Lance et al.[3] obtained in a bubbly homogeneous flow subjected to a constant shear show that the mechanism of redistribution of the turbulence is strongly altered by the presence of bubbles. It is revealed by tendency of turbulence

Correspondence concerning this article should be addressed to A. Line at alain.line@insa-toulouse.fr.

to isotropy and by a sometimes important decrease of the turbulent friction. Generally speaking, the experimental observations obtained in bubbly flows in vertical pipes show an increase of the turbulent fluctuations in weakly sheared zones (in the neighbourhood of the axis of the pipe) while close to walls, where the production of the turbulence by shear flow is important, the effect of bubbles is more complex and can even lead, under certain conditions, to a damping of the turbulence intensity in comparison with the equivalent single phase case. Several authors tried to analyze the mechanisms which control the level and the structure of the turbulence in bubbly flows with the objective to develop adequate models to represent these phenomcna.[3–6] These analyses attempted to specify the dominant phenomena which play a role in the structure of the two-phase turbulence. These studies have indicated that the structure of turbulence in bubbly flows results from a competition between several phenomena, the most important ones being the production, the dissipation, the damping by bubbles, and the redistribution. The production of the turbulence is associated with two processes: the turbulence induced by the shear flow, as for single phase flows, is produced by the average gradients of velocity and turbulence can also be produced by the fluctuating movement of bubbles. The turbulence produced by the fluctuating movement of bubbles increases considerably the turbulence in the flows with weak average gradients (grid turbulence, inside kernels of shear flows, and external boundary layers). On the other hand, measurements in bubbly flows in pipes show that the turbulent stress can be either more or less important than in single phase flow. The dissipation of the turbulence, when it increases, can induce a reduction of the turbulence, as observed in certain shear flows.[6] Indeed, the wakes of bubbles can contribute to an increase of the dissipation. Nevertheless, the experiments of homogeneous turbulence of Lance and Bataille[1] indicate that there is a balance between production and dissipation in the wakes of bubbles. Through an analysis of the characteristic time scales of production, transfer, and dissipation of the turbulent kinetic energy, these authors show that the energy produced in the wakes of bubbles is directly dissipated before its transfer takes place. The redistribution between the diagonal components of the Reynolds stress tensor plays an essential role in the modification of the structure of turbulence in two-phase flows. This was observed in the experiments of Lance et al.[3] on the flow of homogeneous turbulence with constant shear. The experimental results which concern the various components of the Reynolds stress tensor indicate, for a certain shear range, a tendency to isotropy that is more pronounced than in single phase flow together with a significant damping of the turbulent stress. The damping of the turbulence in bubbly flow was also observed in a pipe.[7,8] These authors show that except for the central zone of the flow, the isotropy of the two-phase flow is more pronounced than for the single phase flow accompanied by a decrease of the turbulent shear and sometimes a damping of the turbulent intensity. The experiments of Serizawa et al.[8] indicate that this damping concerns only the longitudinal component that indicates a more important transfer to the other components. On the other hand, an increase of the anisotropy of the turbulence is observed in certain low shear flows as those of homogeneous turbulence[1] or locally in the central zone of the flows in a pipe. The analysis of these situations where the production by the average gradients is weak and where the turbulence in single phase flow is a priori isotropic allows the supposition that the turbulence induced by bubbles, which is fundamentally anisotropic, overlaps in a sheared flow turbulence. Indeed, the experiments of ascending bubbles in a stagnant liquid indicate that in the absence of turbulent shear flow, the turbulence induced by bubbles is anisotropic.[9,10] In a general way, the mechanisms which control the turbulence in bubbly flows are far from being independent. Their consideration in the closure laws of the transport equations of the turbulent variables leads, as we will see later, in remarkable improvements of the closure of the turbulence. In terms of turbulence modeling in bubbly flows, there are the models using a single time scale. It means that, in this kind of models, we do not proceed to the decomposition between the turbulent fluctuations produced by shear and those produced by bubbles.[11–15] Among these models, one can distinguish the models derived to the first order and the models derived to the second order. There are also models which adopt two time scales, to differentiate between two types of fluctuations. These models may include an implicit or explicit decomposition of the turbulence which associates with Reynolds tensor a ''turbulent'' part and a ''pseudo-turbulent'' part due to bubbles.[3,5,6,16–19] The role of the turbulence in the migration of bubbles in bubbly flows in vertical pipes was mentioned by Drew and Lahey.[20] By neglecting all the interfacial forces, these authors established analytically an expression which relates the radial distribution of phase fraction with the pressure gradient. As the transverse pressure gradient becomes dependent on the turbulence, Drew and Lahey[20] managed to connect the distribution of the phase fraction with the structure of the turbulence of the continuous phase. This formulation allowed reproducing the trends of distribution of the phase fraction, in particular, in terms of the peak of phase fraction close to the wall.

The experiments of bubbly flows in a pipe under microgravity conditions[21] show that this formulation is incomplete since in microgravity the profiles of phase fraction are inverted without the profiles of turbulence being modified. As in microgravity the interfacial exchange associated with the average relative velocity is weak, this result opens the question of the role of the turbulent contribution of the interfacial exchange on the distribution of the phase fraction in bubbly flows. In their experiments of bubbly flow with in a sudden extension, Bel F'dhila[22] and Bel F'dhila and Simonin[23] managed to establish experimentally that the transverse balance assessments of momentum cannot be closed if we consider only the average contributions of the terms of interfacial exchange of momentum. Thus, they showed the importance of the turbulence terms stemming from the average of the interfacial terms in the exchange of momentum and consequently in the resulting distribution of the phase fraction.

Generally speaking, the two fluid models, at least in their usual formulations, do not take into account in a clear way the turbulence terms stemming from the average of the terms of interfacial exchange, even if certain modeling works tried to introduce in a more or less precise way these contributions. Several modeling works suggest introducing the

turbulent contributions of the interfacial transfer of momentum in terms of a dispersion term which should be proportional to the gradient of phase fraction.[24,25] Others focus on the turbulent contribution of the added mass.[23,26] The model proposed by Chahed et al.[26] will be discussed in this article and compared with experimental data acquired in an air-lift reactor.

The Eulerian two-fluid model will be used in this study. It constitutes an effective tool to predict the characteristics of the hydrodynamics of these reactors. There are several works in the literature which were interested in the Eulerian modeling of these gas-liquid reactors. One of the first works dedicated to bubble columns is that of Sokolichin and Eigenberger.[27] This analysis of bubble columns was followed by several works.[28–30] In the past, airlift reactor modeling has been performed at different levels. First, global empirical correlations have been developed[31] and global models have been proposed.[32] Then, local analysis based on numerical simulations has been developed. In a review, Merchuk[69] mentioned only three works using CFD for airlift reactors: Cockx et al.[33,34] and Mudde and van den Akker.[35] In Cockx et al.,[33,34] the ASTRID code was used. It was the first attempt at modeling bubbly flow in an airlift reactor, based on a local two-fluid model. However, the closure relation for momentum interfacial transfer was limited to drag. Mudde and van den Akker[35] used a very similar model but their validation of the model was limited to global gas fraction. Since then, Van Baten et al.,[36] Oey et al.,[37] and Talvy et al.[38,39] presented CFD works to describe hydrodynamics of internal loop airlift reactors. The simulations of Van Baten et al.[36] were based on the CFX code. In their Eulerian approach, these authors modeled the interfacial transfer of momentum in terms of drag, without added mass effects and without gas bubble turbulent dispersion. Good agreement between simulations and experiments was obtained in terms of global gas hold up and global liquid circulation. Oey et al.[37] presented numerical simulations of an oscillating internal loop airlift reactor. 3-D simulations were performed using an Eulerian two-fluid approach. The interfacial transfer of momentum was modeled in terms of drag, including the classical added mass effect. The authors focused on transient phenomena and compared the predicted period of oscillations in the downcomer with experimental values. Talvy et al.[38,39] presented numerical simulations obtained with the Fluent code. Gas bubble dispersion was accounted for in terms of a drift velocity which was shown to play a key role in the simulations. The validation of the simulations was discussed in terms of global values (global gas hold up in the riser and downcomer and global liquid circulation). In addition, the validation included comparison of longitudinal profiles of gas fraction in the riser and the downcomer as well as transversal profiles of the liquid velocity in the nonaerated part of the downcomer. This last study, which included mass-transfer modeling, concluded on the existence of significant spatial heterogeneity of oxygen concentration in the gas.

The object of this article is to discuss closure laws of momentum transfer related to gas dispersion in the airlift configuration. Without lift force and without turbulent added mass term, the bubbles move toward regions where the turbulence is high and the pressure is low. Lift can counterbalance the pressure gradient only in the case where the velocity gradient has the same sign as the pressure gradient (or the turbulence gradient). Furthermore, modeling of the lift force remains controversial. When the turbulent added mass contribution is introduced in the model, the bubble migration toward the low pressure region can be counter-balanced and the void fraction profile can thus be significantly modified. In this article, we illustrate and discuss the sensitivity of the simulation to momentum transfer modeling to highlight the role of the turbulent contribution of the added mass to predict the dispersion of gas bubbles in a two-fluid model. The pilot geometry retained in this study is an internal loop airlift reactor. The CFD code used for performing numerical simulations is MELODIF.

We first present the two-fluid model, highlighting the main closure formulations, on both turbulence and exchange of momentum between gas and liquid. Different models of exchange of momentum between gas and liquid are discussed. The model proposed by Chahed et al.[26] including the influence of the turbulent part of added mass force is presented. This model includes no lift, no drift velocity and no turbulent dispersion term.

This model is tested in the airlift reactor and compared with a data bank obtained for this study. Subsequently, a sensitivity analysis to the parameters of the model is presented and discussed. In our experiments, air bubbles are injected in the airlift reactor by means of a membrane; the size distribution of injected bubbles is thus almost mono-dispersed. Because of low gas fractions and low shear, both coalescence and break-up effects are non dominant. Consequently, in this study, focusing on momentum transfer in two-fluid model, the bubble diameter will be fixed at the inlet and considered to remain constant. In addition, this study is limited to bubbly flow pattern and low gas fraction; churn flow is out of the scope of this article.

Two-Fluid Model: Averaged Equations and Closure Issues

We denote the local void (gas) fraction as α and we define, for each instantaneous variable Φ, the mean and fluctuating values, respectively, $\overline{\overline{\Phi}}$ and Φ' in the liquid phase; the variables related to the gas phase have the subscript G. For incompressible bubbly flow, without interfacial mass transfer, the average continuity equations in the liquid and in the gas, respectively:

$$\frac{\partial(1-\alpha)}{\partial t}+\frac{\partial}{\partial x_i}\left[(1-\alpha)\overline{\overline{u_i}}\right]=0 \tag{1}$$

$$\frac{\partial \alpha}{\partial t}+\frac{\partial}{\partial x_i}(\alpha\overline{\overline{u_{Gi}}})=0 \tag{2}$$

where $\overline{\overline{u}}_i$ and $\overline{\overline{u}}_{Gi}$ are the liquid and the gas velocity components respectively.

The averaged equations of momentum in the liquid and in the gas are written for turbulent bubbly flows (the viscous stress tensors are neglected in comparison with the turbulent correlations):

$$\rho(1-\alpha)\frac{D\overline{\overline{u_i}}}{Dt}=-(1-\alpha)\frac{\partial\overline{\overline{p}}}{\partial x_i}-\rho\frac{\partial}{\partial x_j}[(1-\alpha)\overline{\overline{u_i'u_j'}}]+\rho(1-\alpha)g_i-\alpha M_{Gi} \tag{3}$$

$$\rho_G \alpha \frac{d\overline{\overline{u_{Gi}}}}{dt} = -\alpha \frac{\partial \overline{\overline{p}}}{\partial x_i} - \rho_G \frac{\partial}{\partial x_j}[\alpha \overline{\overline{u'_{Gi} u'_{Gj}}}] + \rho_G \alpha g_i + \alpha M_{Gi} \quad (4)$$

where $\frac{D}{Dt} = \frac{\partial}{\partial t} + \overline{\overline{u}}_j \frac{\partial}{\partial x_j}$ and $\frac{d_G}{dt} = \frac{\partial}{\partial t} + \overline{\overline{u}}_{Gj} \frac{\partial}{\partial x_j}$ are the material derivatives following the liquid and gas phases, respectively, $\overline{\overline{p}}$ is the pressure, ρ and ρ_G are the liquid and gas densities, respectively.

The set of Eqs. 1–4 constitutes the classical two-fluid model. Solving the system requires the expression of closure relations on turbulent stresses in the liquid, $\overline{\overline{u'_i u'_j}}$, on turbulent terms related to the gas phase, $\overline{\overline{u'_{Gi} u'_{Gj}}}$ and on the interfacial momentum transfer, M_{Gi}. These different closure points are addressed in the following. In this article, we mainly focus on the modeling of interfacial transfer of momentum, to reproduce the dispersion of the gas. In fact, turbulence modeling cannot be ignored. In particular, the closure of turbulent correlation in the gas phase, $\overline{\overline{u'_{Gi} u'_{Gj}}}$, appears to play a key role not only in the momentum equation of the gas but also in the momentum transfer term.

Turbulence modeling in two-fluid model

In the two fluid model (Eq. 1–4), there appear two kinds of turbulent stress, the classical Reynolds stress tensor components in the continuous liquid phase, $\overline{\overline{u'_{Gi} u'_{Gj}}}$ and a turbulent term related to the dispersed gas phase, $\overline{\overline{u'_{Gi} u'_{Gj}}}$. In this work, the turbulent viscosity concept will be retained to close the Reynolds stress tensor in the liquid phase:

$$-\overline{\overline{u'_i u'_j}} = V_t \left(\frac{\partial \overline{\overline{u_i}}}{\partial x_j} + \frac{\partial \overline{\overline{u_j}}}{\partial x_i} \right) - \frac{2}{3} k \ \delta_{ij} \quad (5)$$

where V_t is the turbulent kinematic viscosity and k is the turbulent kinetic energy, per unit mass, in the liquid phase. A basic problem of such a modeling consists in accounting for the effect of dispersed gas phase (bubble) on the structure of the turbulence in the continuous liquid phase.

Sato and Sekoguchi[40] were the first to propose accounting for bubble effect on turbulence by adding linearly a bubble induced viscosity to the turbulent viscosity. The added viscosity induced by bubble displacement was expressed in terms of bubble diameter d and the magnitude of the relative velocity between the gas and the liquid. Lopez de Bertonado et al.[12] followed this pioneering work. In their work, the kinetic energy induced by bubbles is calculated by a transport equation, referring to asymptotic values of the kinetic energy induced by bubbles estimated from potential flow theory.

Nevertheless, experiments concerning homogeneous uniformly sheared bubbly flow[3] indicate that the turbulence in bubbly flow can be more isotropic than in single phase flow; thus, a significant reduction of the turbulent shear can be observed, in comparison with the equivalent single-phase flow. In terms of turbulence modeling, these experimental results suggest that a second-order turbulence closure model should be needed to take into account the effect of the bubbles on the redistribution mechanisms between the normal components of the Reynolds stress tensor. Chahed et al.[18,26] developed such a second-order turbulence model, in which the Reynolds stress tensor of the continuous liquid phase was separated into two parts: a turbulent part, produced by the gradient of mean velocity and a pseudo-turbulent part, induced by bubble displacements; each part was determined by a transport equation. The transport equation for the turbulent part of the Reynolds stress tensor was modeled as in single phase flow; a supplementary effect of the bubbles was introduced in the closure of the redistribution and diffusion terms. The reduction of the second-order turbulence closure provided an original formulation of the turbulent viscosity in bubbly flows that will be tested in an airlift reactor in this article. This turbulent viscosity can be written as:

$$V_t = V_{t0} \frac{(1 + \frac{k_s}{k_0})}{(1 + \alpha \frac{\tau_t}{\tau_s})} \quad (6)$$

where v_{t0} is the classical turbulent viscosity, k_0 is the turbulent part of kinetic energy, k_s is the pseudo-turbulent part of kinetic energy, τ_t is a characteristic time scale related to the vortex stretching, and τ_s is a characteristic time scale related to bubble (size and relative velocity). The relation (6) for the turbulent viscosity exhibits interesting trends. When the pseudo-turbulent part of the kinetic energy k_s is large in comparison with the turbulent part k_0, the turbulent viscosity can be increased. It is particularly the case in bubbly flows where the amount of bubble-induced turbulence is important, such as in mixing layer and bubbly wake experiments. Roig et al.[2] On the contrary, when the shear induced turbulence is rather important as in highly sheared bubbly flows, the effect of the supplementary stretching may be a source of turbulent viscosity decrease. Thus, a turbulent viscosity decrease may occur when the ratio between the bubble-induced turbulence and the shear-induced turbulence is sufficiently weak (for instance: $\frac{k_s}{k_0} < \alpha \frac{\tau_t}{\tau_s}$). It is, for example, the case of the experiments of homogeneous shear bubbly flow.[3] The analysis of the turbulence structure in this bubbly flow showed that the turbulent viscosity closure (Eq. 6) succeeded in reproducing the reduction of the turbulent shear stress observed in bubbly flows in comparison with the equivalent single phase flow.[19] In two-phase flow reactors, the gas-liquid hydrodynamic interactions are strong and turbulent mixing can be significantly modulated by the pseudo-turbulence induced by the bubbles. The coupling between the continuous phase (liquid) and the dispersed one (gas bubbles) controls the interfacial transfers. Turbulence and pseudo-turbulence are basically two different phenomena associated to different scales. Turbulence models based on the separation of turbulence and pseudo-turbulence contributions lead to an improved description of the two-phase turbulence structure, in particular, in bubble-columns or airlifts, where the structure of the flow is governed by buoyancy effects and the role of the bubble induced turbulence is of great importance.

The turbulence closure is based on the turbulent viscosity issued from second order turbulence closure (Eq. 6). This turbulent viscosity is generated using a three equation turbulence model.[18] The transport equations of the three equation turbulence model have been modeled as follows:

$$\frac{D}{Dt} k_0 = \frac{C_{sk}}{(1-\alpha)} \frac{\partial}{\partial x_j} \left[(1-\alpha)(\tau_t k_0 + \tau_b k_S) \frac{\partial k_0}{\partial x_j} \right] + V_t \frac{\partial \overline{\overline{u_i}}}{\partial x_j} \left(\frac{\partial \overline{\overline{u_i}}}{\partial x_j} + \frac{\partial \overline{\overline{u_j}}}{\partial x_i} \right) - \varepsilon_0 \quad (7)$$

$$\frac{D}{Dt}k_S = \frac{C_{sk}}{(1-\alpha)}\frac{\partial}{\partial x_j}[(1-\alpha)(\tau_t k_0 + \tau_s k_S)]\frac{\partial k_S}{\partial x_j} + \frac{1}{4}\frac{D}{Dt}\alpha\| \vec{u_R} \|^2 \tag{8}$$

$$\frac{D}{D_t}\varepsilon_0 = -\frac{C_{s\varepsilon}}{(1-\alpha)}\frac{\partial}{\partial x_i}\left(\frac{k_0}{\varepsilon_0}(1-\alpha)\overline{\overline{u_k' u_l'}}\frac{\partial \varepsilon_0}{\partial x_k}\right) + \frac{\varepsilon_0}{k_0}\left(-C_{1\varepsilon}\overline{\overline{u_i' u_k'}}\frac{\partial \overline{U_i}}{\partial x_k} - C_{2\varepsilon}\varepsilon_0\right) \tag{9}$$

The diffusion term closure is based on second-order turbulence modeling and has been split into "turbulent" and "pseudo-turbulent" contributions. According to this decomposition, the diffusion term includes the equivalent single-phase turbulent effect $C_{s\phi}\tau_t k_0 = \frac{\nu_{t0}}{\sigma_\phi}, (\nu_{t0} - C_\mu \frac{k_0^2}{\varepsilon_0})$ and a supplementary effect due to the bubble motion, $\frac{\nu_b}{\sigma_\phi} = C_{s\phi}\tau_s k_s \approx \frac{C_b}{\sigma\phi}\alpha\, d_b||\vec{u_R}||$ It should be observed that turbulence and pseudo-turbulent diffusion contributions are also related to specific time scales related to the vortex stretching and to the bubble size and relative velocity.

It should be recalled that the total turbulent energy k is thus defined as the sum of the pseudo-turbulent and turbulent parts, and τ_t and τ_s are two characteristic time scales related to the turbulence and to the bubble motion, respectively. The characteristc time scale of bubbles is expressed in terms of bubble diameter d_b and relative velocity as follows:

$$\tau_s = C_R \frac{d_b}{\| \vec{u_R} \|} \tag{10}$$

and the characteristic time scale of turbulence (vortex stretching) is classically based on turbulent kinetic energy and its dissipation rate ϵ_0:

$$\tau_t = \frac{k_0}{\varepsilon_0} \tag{11}$$

The coefficient C_R has been adjusted from the experimental data of uniformly sheared homogeneous turbulence and its value has been fixed to $C_R = \frac{2}{3}$,.[18]

The modeling of the turbulent terms related to the gas phase, $\overline{\overline{u_{Gi}' u_{Gj}'}}$ constitutes a less classical issue. An elegant method to estimate this term should be to write and solve its transport equation. Another approach, a simpler one, is to compare the turbulent gas velocity correlations $\overline{u_G'^2}$, $\overline{v_G'^2}$, $\overline{u_G' v_G'}$ to the liquid ones $\overline{u}'^2$, $\overline{v'^2}$, $\overline{u'v'}$. Tchen[41] was the first to consider the dispersion of particles (small size, spherical shape, and solid phase) in a turbulent field. His analytical derivation of the trajectory of a solid particle was based on a lot of restrictive assumptions. In this first theory (refered to as the Tchen-Hinze theory), the following relations between the turbulent gas velocity covariance and the Reynolds stress tensor in the liquid was obtained:

$$\overline{u_{Gi}' u_{Gj}'} = C_{\text{Tchen-Hinze}}\overline{u_i' u_j'} \tag{12}$$

The detailed expression of the coefficient $C_{\text{Tchen-Hinze}}$ is not reported here, but will be introduced in the discussion section of this article. The Tchen-Hinze coefficient depends on a ratio η of characteristic time scales of the turbulence τ_t and of the bubble τ_s. Thus, one can consider two asymptotic trends for the parameter η. For small values of η, ($\tau_t \ll \tau_s$), the Tchen-Hinze coefficient is close to 9, whereas for large values of η, the Tchen-Hinze coefficient is close to unity. Deutsch,[42] following Csanady,[43] proposed an extension of Tchen- Hinze theory accounting for crossing trajectory effects. However, it is important to emphasize that Tchen- Hinze's theory is only valid for dispersed two-phase flows transporting particles with small sizes in comparison with the smallest turbulent fluctuation scales (Kolmogorov micro-scale). In the case of bubbly flow, the hypothesis of small particle size may often not be-valid. Thus, bubbly flows may require a more complex model, to represent the turbulent fluctuations of the dispersed phase as a function of the turbulent fluctuation of the continuous phase. In a first step of analysis of the weight of interfacial transfer modeling on phase distribution in an airlift reactor, we will assume a simple proportionality relation. Thus, we propose to substitute in Eq. 12 the following expression:

$$\overline{\overline{u_{Gi}' u_{Gj}'}} = C\,\overline{\overline{u_i' u_j'}} \tag{13}$$

to highlight the effect of these turbulent correlations on the momentum transfer and thus on the phase distribution of the gas. The main issue of this article is to highlight the role of turbulent contribution of added mass in the modeling of gas dispersion. It is not to model C but to analyze the sensitivity of numerical results to the value of C to estimate the order of magnitude of this coefficient C, which relates turbulent correlations in the gas to the Reynolds stress in the liquid. Of course, the range of magnitude of C is based on the expression proposed by Deutsch and derived from Tchen theory.

Interfacial momentum transfer modeling

Before addressing the closure issue of the interfacial momentum transfer, it is instructive to better understand the hydrodynamics of airlifts reactors. Indeed, in such a reactor, the two-phase flow is mainly controlled by momentum balance, Eqs. 3 and 4. Neglecting acceleration and gas weight compared with the force exerted by the liquid on the gas, Eq. 4 indicates that the resulting force on the bubbles is zero:

$$-\alpha\frac{\partial \overline{\overline{p}}}{\partial x_i} + \alpha M_{Gi} \approx 0 \tag{14}$$

Combining the momentum equations of the liquid and of the gas (3) and (4), the two-fluid model may be rewritten in a different form. With the simplified form of the momentum equation for the gas (Eq. 14), the momentum equation of the gas-liquid mixture becomes:

$$\rho(1-\alpha)\frac{D\overline{\overline{u_i}}}{Dt} = -\frac{\partial(\overline{\overline{p}} + \rho\, g\, x_i)}{\partial\, x_i} - \frac{\partial}{\partial\, x_i}\left[\rho(1-\alpha)\overline{\overline{u'_i u'_j}}\right] + \rho\,\alpha\, g_i \tag{15}$$

Equation 15 indicates that the motion of the liquid phase is similar to that of a single-phase flow in the presence of a buoyancy force $\alpha\rho g$. This expression highlights the effect of buoyancy, which is a characteristic behaviour of airlift reactors

as well as bubble columns. In such bubbly flows, the void fraction distribution determines the hydrodynamics of the reactor. Thus, accurate modeling of the interfacial momentum transfer, which controls the local bubbles distribution through the reactor, is particularly important for suitable prediction of such buoyancy driven bubbly flows. Therefore, the main issue of this article is to analyze gas dispersion modeling.

The interfacial momentum transfer term is usually modeled as the average force exerted by the liquid on the bubbles. Based on the analysis of pipe bubbly flow under microgravity conditions, Chahed et al.[26] showed that the turbulent contribution in the momentum transfer was important. They proposed to reconsider the turbulent term due to the added mass force in the formulation of the interfacial term. Lift force is neglected in this work, and no additional term of turbulent dispersion needs to be introduced. The interfacial transfer of momentum is modeled as follows:

$$M_{Gi} = -\rho \frac{\overline{\overline{u_{Ri}}}}{\tau_b} - C_A \rho \left(\frac{d_G \overline{\overline{u_{Gi}}}}{dt} - \frac{D\overline{\overline{u_i}}}{Dt}\right) - \frac{C_A}{\alpha} \rho \frac{\partial}{\partial x_j} \left(\overline{\overline{\alpha u'_{Gi} u'_{Gj}}} - \overline{\overline{\alpha u'_i u'_j}}\right) \tag{16}$$

where $\overline{\overline{u_R}}$ is the relative velocity of the bubbles.

The interfacial averaged force contains, respectively, drag force (term with a characteristic time scale τ_b), added mass force (first term with a coefficient C_A), and a specific turbulent term issued from the averaging of the added mass force (second term with a coefficient C_A). The main originality of this expression is due to the formulation of the interfacial force especially concerning the derivatives involved in the added mass force. The different terms involved in momentum transfer will be shortly discussed.

Drag.

The momentum transfer induced by the drag is expressed as follows:

$$M_{Gi}^{D} = -\rho \frac{\overline{\overline{u_{Ri}}}}{\tau_b} \tag{17}$$

The bubble time scale τ_b is defined as follows:

$$\tau_b = \frac{4}{3} \frac{4_b}{C_D \left\| \vec{u}_R \right\|} \tag{18}$$

where C_D is the drag coefficient. Bel F'dhila and Duineveld[44] found a good correspondence between experimental values of the drag on a bubble in contaminated water by using the expression of the drag coefficient C_D for rigid spheres with large values of Reynolds numbers between 50 and 200.[45] The effect of the contamination of the water makes the bubble rigid so that its drag is comparable to that of a rigid sphere. Zuber and Ishii[46] proposed a correlation which takes into account this phenomenon by expressing it in terms of the Eötvös number that represents the relationship between buoyancy and the effects of the superficial tension. The expression proposed by Zuber and Ishii[46] for distorted bubbles is given by:

$$C_D = \frac{2}{3} E_0^{1/2} \tag{19}$$

where the Eötvös number is defined as:

$$E_0 = \frac{\Delta\rho \; g \; {d_b}^2}{\sigma} \tag{20}$$

For a bubble size of 3–4 mm, the drag coefficient is close to unity, as expected after Talvy et al.[38]

Added Mass. The momentum transfer induced by the added mass is expressed as follows:

$$M_{Gi}^{AM} = -C_A \rho \left(\frac{d_G \overline{\overline{u_{Gi}}}}{dt} - \frac{D\overline{\overline{u_i}}}{Dt}\right) \tag{21}$$

where C_A is the added mass coefficient, equal to 0.5. Several authors[33,37] considered that, in a steady-state and fully developed flow as it is the case in airlift reactor (at least far from the gas injector), the effect of the added mass force is weak in comparison with the mean drag force. In unsteady flows, Leon Bécerril and Liné[47] showed that the added mass term was essential to initiate the instability phenomena occurring at the transition between homogeneous and heterogeneous flow in bubble columns. In particular, in such a heterogeneous regime, local accelerations occur and the added mass force can become significant with regard to the drag. In addition, the turbulent fluctuations of the added mass force may result in an average effects that certain authors analyzed and that turns out to be determining in some typical bubbly flows (two-phase flow with bubbles in an abrupt extension, Bel F'Dhila[22] and micro-gravity experiments, Chahed[5])

Turbulent Contribution of Added Mass. In this work, the momentum transfer induced by the turbulent contribution of the added mass is expressed as follows:

$$M_{Gi}^{TAM} = \frac{C_A}{\alpha} \rho \frac{\partial}{\partial x_j} \left(\overline{\overline{\alpha u'_{Gi} u'_{Gj}}} - \overline{\overline{\alpha u'_i u'_j}}\right) \tag{22}$$

Given the relation between the turbulent terms related to the gas phase, $\overline{\overline{u'_{Gi} u'_{Gj}}}$ and the Reynolds stresses in the liquid (Eq. 13), one can write:

$$M_{Gi}^{TAM} = -\frac{C_A}{\alpha} \rho \frac{\partial}{\partial x_j} \left[\alpha (C-1) \overline{\overline{u'_i u'_j}}\right] \tag{23}$$

Turbulent Dispersion. Several modeling works adopted the formulation of a turbulent contribution of the interfacial transfer.[48–51] These models where the turbulent dispersion is proportional to the gradient of void fraction were reviewed by Moraga et al.[52] However, the simulations of bubbly flows under microgravity conditions[26] indicate that this modeling is insufficient as it cannot reproduce the inversion of the profile of void fraction which is observed in microgravity. No turbulent dispersion term will be included in the present work.

Lift. By definition, it is the orthogonal force at the slip velocity and it takes into account the radial displacement of the bubble induced by its rotation around its axis. Numerical works[53,54] show that the lift coefficient depends strongly on

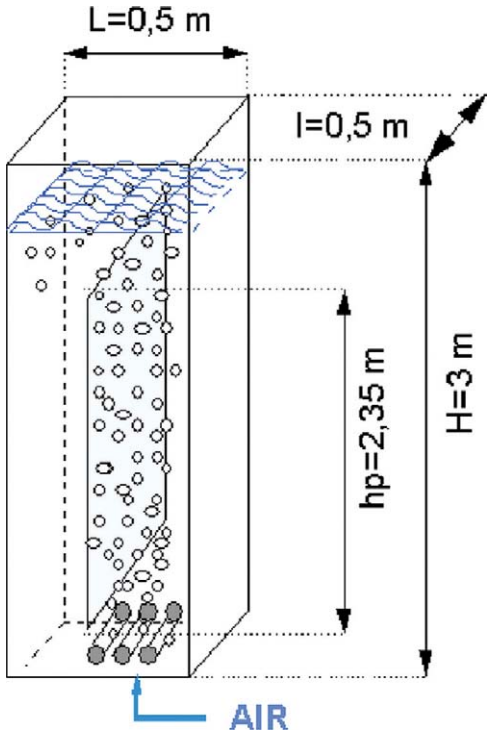

Figure 1. Airlift internal loop reactor.

[Color figure can be viewed in the online issue, which is available at wileyonlinelibrary.com.]

the value of Reynolds number and on the size of the bubble, so that it can take negative values below a certain size. The modeling of the lift force has been discussed by Sokolichin et al.[55] The authors pointed out that the lift force has been used as a parameter improving the simulations without basic justifications. Consequently, the lift force will be neglected in the following.

Experiments

Airlift reactor

The internal loop airlift reactor is a parallelepiped vessel of 3 m height and 0.5 m width and depth (Figure 1). It is equipped with an internal baffle, located in its middle (h = 2.35 m high). The baffle position is fixed (150 mm above the bottom). The reactor is initially filled up with tap water, up to 2.6 m high. The pilot can be divided in four sections: an upward flow aerated section (the riser), the free surface flow above the internal wall, a downward flow less aerated section (the downcomer), and the flow below the internal wall, including the gas injector, usually called sparger. The global liquid circulation is induced by air injection, which is maintained by horizontal cylindrical membrane spargers (Flexazur T415 membrane covering Plexiglas cylinders), located at the bottom-right of the reactor. The outside diameter of each cylindrical membrane sparger is 40 mm. The axis of the cylindrical membrane spargers is located at 100 mm above the bottom of the pilot. The injectors being made from a perforated membrane, the bubble diameters are calibrated by the superficial gas velocity. The superficial gas velocity is equal to 1.7 cm/s and is the same than the velocity used in the works of Couvert,[56] Cockx,[57] and Talvy et al.[38]

Material and methods

Two classical techniques are used in this study to characterize the two-phase flow in the airlift reactor. The hot wire anemometer enables to measure the mean and fluctuating components of the liquid velocity and the optical bi-probe measures the gas holdup and the bubble velocity.

The hot film anemometer is used to measure the velocity of the liquid phase. In this study, it is composed of a single cylindrical hot film probe (Dantec, 55R11) and a constant temperature anemometer (Dantec). A National Instruments data card permitted to acquire the signal of the film with a frequency selected to be 10 kHz and measurements were recorded for 75s. It should be recalled that the passage of a bubble on the film causes a sudden change in heat transfer, represented by a succession of high and low peaks in the signal of the voltage recorded by the data acquisition card (Figure 2a). A phase discrimination algorithm described by Farrar and Bruun[58] and developed by Larue de Tournemine[59] permitted to eliminate the portion of the signal related to the bubble passage, and finally, we obtain a signal associated only to the instantaneous liquid velocity (Figure 2b).

A double optic probe (RBI) is also used in this experiment. Infrared light, generated by an opto-electronic module is transmitted into each glass fiber. Considering the difference of refractive index between air and water, when liquid wets a probe tip the light is refracted whereas when a gas bubble passes through the probe it is reflected. Thus, after data processing, the signal is binarized[3,8,60,61] for a description of the signal processing algorithms): a value equal to 1 corresponds to the gas phase and 0 for the liquid. One obtains an experimental Heaviside function accounting for the occurrence of gas phase at a given point. Thus, one can estimate the local gas fraction by ensemble averaging. The diameter of the optical fiber is one-order of magnitude smaller than the bubble size (bubbles of several millimeters); thus, most of the bubbles are pierced by the optical probe and deflected effects are small.

In addition, two optical probes are used. Their tips are distant by 0.001 m. National Instruments data card connected

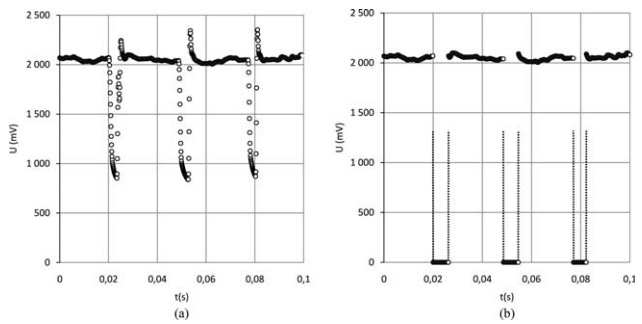

Figure 2. (a) Raw signal of hot wire anemometer in bubbly flow; (b) processed signal of hot wire anemometer in bubbly flow.

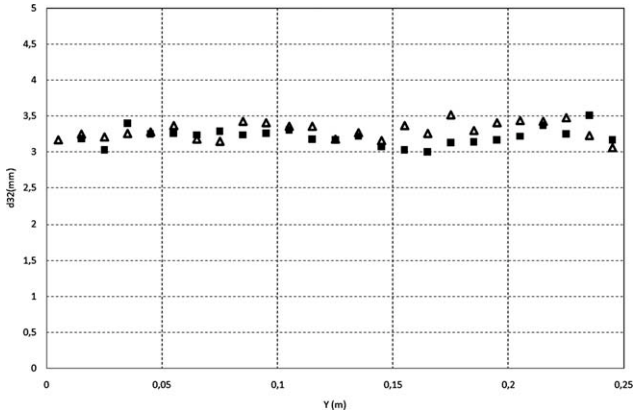

Figure 3. Experimental profile of d_{32} bubble diameter at different heights in the airlift reactor (■ H = 2.12 m, △ H = 1.24 m).

to the computer enables to acquire the signal of the two probes with a frequency chosen equal to 10 kHz. To calculate the bubble velocity, it is necessary to estimate the flight time between the two probe tips. Thus, one must associate the front of a given bubble in the two signals. Inter-correlation function is performed to determine this time scale. Finally, we can calculate the mean velocity of individual bubbles. Statistical is then necessary to estimate the average value of gas bubble velocity.

The d_{32} diameter has been statistically determined. Horizontal profiles of the statistical d_{32} diameter are plotted on Figure 3 for two different heights (H = 1.24 m and 2.12 m). It can be seen that there is no significant evolution of d_{32} diameter in the horizontal direction or in the vertical direction. Therefore, the mean diameter of the bubbles will be considered as constant in the simulations, coalescence, and breakup being neglected. One can recall that the size of the bubbles injected in the airlift reactor can be estimated to be close to 3.5 mm.[62]

The experimental distribution of bubble cords is plotted on Figure 4. These measurements confirm that the membrane injector generates monodispersed bubbles. Figure 3 showed that the Sauter diameter is close to 3.5 mm. It is clear from the Figure 4 that the maximum diameter of the bubbles is between 4.5 and 5 mm. One can recall that for spherical bubbles with a volume $\frac{4}{3}\,\pi\,r_b^3$ and a projected area (normal to the probe) equal to $\pi\,r_b^2$, the average chord is equal to the ratio volume over projected surface and is thus equal to $\frac{4}{3}\,r_b = \frac{2}{3}\,d_b$. Consequently, given a bubble diameter equal to 3.5 mm, the average size of cord for a spherical bubble would be close to 2.3 mm, which is consistent with Figure 4.

Numerics

The closure of turbulence and interfacial forces have been implemented in the code MELODIF and applied to various various bubbly flow configurations, e.g., grid and pure shear flows, mixing layer, and wake flows, Bellakhel[63] and Ayed et al.[64] Melodif is a two-dimensional Eulerian code developed by EdF.[23,65–67] It is based on finite difference discretisation and applied to the simulation of the air lift The numerical results are compared with the experimental data and the analysis is focussed on the turbulence dispersion on the dispersed phase. The computational domain is a 2-D grid with 134 longitudinal nodes and 27 transverse nodes. The domain describes the experiment loop. It has a vertical length of 2.68 m and a transverse length of 0.25 m in the riser as well as in the downcomer. Wall conditions are applied at the solid boundaries. The inlet section corresponds to gas injection position were the void fraction and the gas velocity injection are fixed according to the experimental gas flux. The bubble diameter is set equal to 3.5 mm, which represents the average bubble diameter observed in the experiments.

Results and Discussion

Choice of simulation test cases

Consider the simplified case of quasi-parallel 2-D flow. As in single-phase flow, the transverse acceleration of both liquid and gas are negligible in vertical 2-D flow in comparison with the pressure and turbulence gradients. The liquid velocity components being noted u, v in the vertical (x) and in the horizontal (y) direction, respectively, the transverse momentum equations in the liquid can be reduced to:

$$0 = -\frac{\partial}{\partial y}\left[\overline{\overline{p}} + \rho(1-\alpha)\overline{\overline{v'^2}}\right] \tag{24}$$

Accounting for the previous Eq. 14 in the gas phase, one can write:

$$\frac{\partial}{\partial y}\left[\rho(1-\alpha)\overline{\overline{v'^2}}\right] + M_{Gy} = 0 \tag{25}$$

Following the model of Chahed, the momentum transfer term can be derived for this simplified case. The drag contribution, M_{Gy}^D, to the interfacial momentum transfer, M_{Gy}, can be written as

$$M_{Gy}^D = -\rho\frac{v_{Ry}}{\tau_b} \tag{26}$$

where v_{Ry} is the y component of the relative velocity between the gas and the liquid. The added mass term has no mean contribution in fully developed and steady state flow. The y

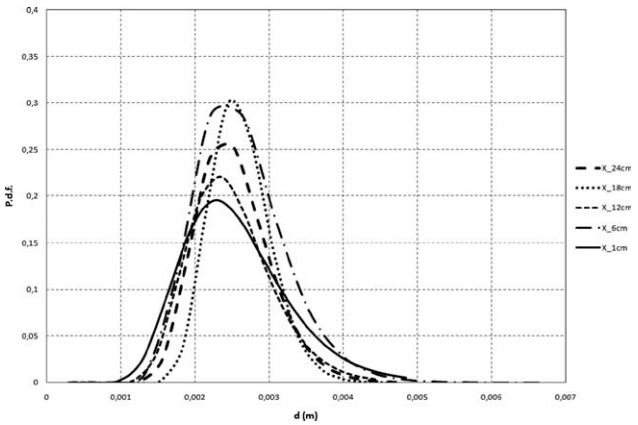

Figure 4. Experimental distribution of bubble chords at height H = 2.12, for different horizontal positions.

component of the turbulent part of the added mass can be written as:

$$M_{Gy}^{TD} = -\frac{C_A}{\alpha}\rho\frac{\partial}{\partial y}\left[\alpha(C-1)\overline{\overline{v'^2}}\right] \quad (27)$$

Then, inserting (26) and (27) in the momentum balance (25), one obtains in terms of horizontal component of the relative velocity:

$$v_{Ry} = \tau_b\left\{\frac{\partial}{\partial y}\left[(1-\alpha)\overline{\overline{v'^2}}\right] - \frac{C_A}{\alpha}\frac{\partial}{\partial y}\left[\alpha(C-1)\overline{\overline{v'^2}}\right]\right\} \quad (28)$$

A first value of the coefficient C to be tested is thus $C = 1$. In this case, the turbulent contribution of the added mass vanishes. Only the drag force is accounted for.

If we develop the r.h.s. of Eq. 28, one can obtain:

$$v_{Ry} = \tau_b\left\{[1-\alpha-(C-1)]\frac{\partial\overline{\overline{v'^2}}}{\partial y} - \left(1+C_A\frac{C-1}{\alpha}\right)\overline{\overline{v'^2}}\frac{\partial\alpha}{\partial y}\right\} \quad (29)$$

Considering diluted systems ($\alpha \ll 1$) and assuming that the added mass coefficient is equal to 0.5, a second value of the coefficient C to be tested is $C = 3$. In this case, the first term on the r.h.s. of Eq. 30 vanishes and only the gradient of gas fraction remains.

Another more complex expression to be tested is the expression proposed by Deutsch.[42]

$$C = C_{Deutsch} = \frac{b^2+\eta_r}{1+\eta_r} \quad (30)$$

The parameter b is defined as follows:

$$b = \frac{1+C_A}{\rho_G/\rho + C_A} \quad (31)$$

In air-water flow, the density ratio is such that b is close to $\frac{1+C_A}{C_A} = 3$. η_r is the ratio of the characteristic time scale of the turbulence seen by the gas phase, denoted τ_{GL}^t and the characteristic time scale of the bubble entrainment by the liquid motion τ_{GL}^F:

$$\eta_r = \frac{\tau_{GL}^t}{\tau_{GL}^F} \quad (32)$$

where τ_{GL}^F is given by

$$\tau_{GL}^F = \tau_b\left(\frac{\rho_G}{\rho_L} + C_A\right) \quad (33)$$

and τ_{GL}^t includes the crossing trajectory effects. It is expressed as

$$\tau_{GL}^t = \frac{\tau_L^t}{\sigma_{kL}}(1+C_\beta\zeta_r^2)^{-1/2} \quad (34)$$

The turbulence time scale τ_L^t is given by

$$\tau_L^t = \frac{3}{2}C_\mu\frac{k}{\varepsilon} \quad (35)$$

and ζ_r is defined as the ratio of relative velocity of the bubbles and r.m.s. turbulence:

$$\zeta_r = \frac{\|\vec{u_R}\|}{\sqrt{2k/3}} \quad (36)$$

Such a crossing trajectory effect accounts for the interaction between bubbles and large turbulent eddies. One must consider the interaction in the direction of the slip velocity between the bubbles and the liquid; in this case, the value of C_β is taken to 0.45, whereas the value is fixed to 1.8 when the interaction occurs in the transversal direction.

Returning to the definition of the Deutsch coefficient, two asymptotic cases can be considered: when the ratio η_r is large compared with unity, the coefficient tends to unity. The value $C = 1$ has already been considered. When the ratio η_r is small compared to unity, the Deutsch coefficient tends to $b^2 = 9$. This last value $C = 9$ will be tested in our simulations. In conclusion, four values of coefficient C will be tested $C = 1$, $C = 3$, $C = 9$, and $C = C_{Deutsch}$.

Results

In the following, the analysis is focused on the role of the turbulence in the void fraction distribution in the air lift. This analysis is based on numerical simulations using the Eulerian-Eulerian two-fluid model. The numerical results are compared with local experiment data.

It should be recalled that the objective of the numerical analysis is to point out the importance of the term related to the turbulent contribution of the added mass force in the momentum balance. As shown by Eqs. 22 and 23, this term comprises the turbulent correlations both of gas and liquid. Indeed, using a dispersion model, one can relate the turbulent correlations of the gas to the turbulent correlations of the liquid. In an attempt to evaluate the importance of these turbulent contributions, three particular situations are tested, with constant values of the coefficient relating the turbulent correlations of the gas phase to that of the liquid one (C = 1,3, and 9). A complementary simulation has been performed using the dispersion of Deutsh model, which is based on Tchen theory. The results obtained with Deutsch model are close to the results obtained with a constant value $C = 3$ and thus will be discussed together. Recall that turbulence isotropy is assumed:

$$\overline{\overline{u'^2}} = \overline{\overline{v'^2}} = \frac{2}{3}k \quad \text{and} \quad \overline{\overline{u_G'^2}} = \overline{\overline{v_G'^2}} = \frac{2}{3}C\,k \quad (37)$$

In the first simulation, the C coefficient is set equal to unity. Thus, the turbulent contribution of the added mass force is omitted. The three other simulations take into account the turbulent contribution of added mass. Two simulations are performed with different constant values of C coefficient ($C = 3$ and $C = 9$). A last simulation takes into accounts the expression of Deutsch ($C = C_{Deutsch}$) given by Eq. 30.

Figures 5a,b concern the longitudinal distributions of the gas fraction averaged in a cross section of the airlift, in the riser and in the downcomer, respectively. The numerical profiles are compared with the experimental data of Couvert.[56] The profile of gas fraction obtained with a constant value of

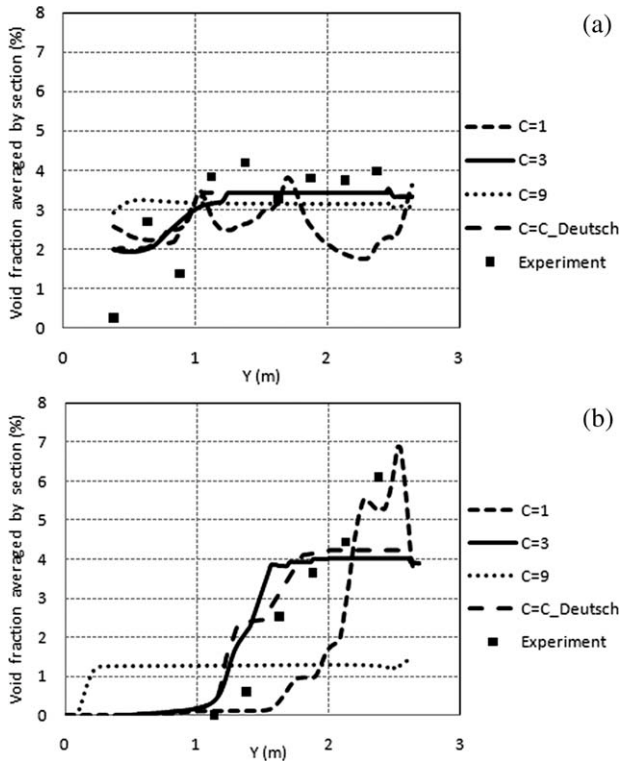

Figure 5. Longitudinal evolution of gas fraction in the: (a) riser compared with the data of Couvert;[56] (b) downcomer compared with the data of Couvert.[56]

the coefficient equal to 3 as well as the profile of gas fraction obtained with a value of the coefficient corresponding to Deutsch proposal are very close to each other (in fact they overlap completely for $1.2 < x < 2.5$) and follow the experimental trends. In the riser, these two numerical profiles reproduce the constant gas fraction 1 m downstream of the sparger, whereas in the dowcomer, the length of the aerated region located in the upper part of the downcomer is well predicted. Increasing the value of the coefficient to 9 overpredicts the dispersion of the gas. The profiles are almost

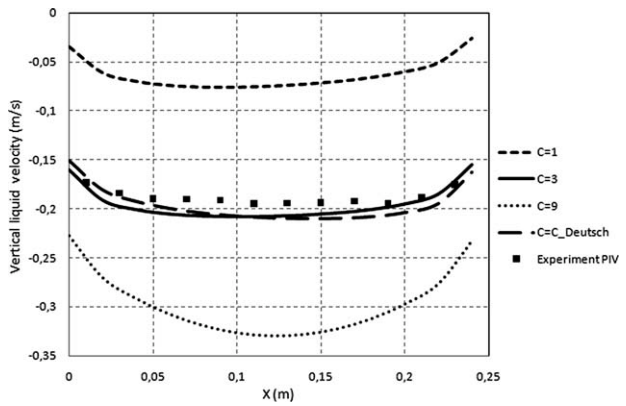

Figure 6. Transversal profile of the vertical component of liquid velocity in the downcomer at a height x = 60 cm above the bottom, compared with PIV experiments.

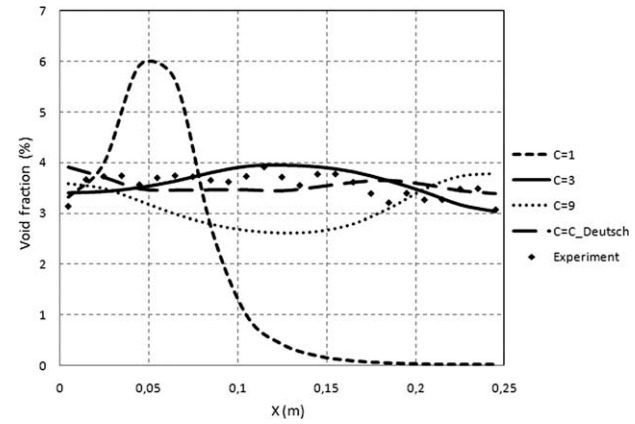

Figure 7. Horizontal profile of void fraction: experiments (full diamonds) compared with simulations.

flat both in the riser and in the downcomer, with a significant overestimation of the aeration of the dowcomer. The smallest value of the coefficient C equal to unity give poor predictions, both in the riser, where the profile of gas fraction is unstable and in the downcomer, where the length of the aerated region located in the upper part of the downcomer is underpredicted.

One can explain some of these trends by comparing, as shown on Figure 6, the simulated values of the liquid velocity in the lower part of the downcomer to PIV profile obtained by Cockx.[57] Here again, there is a very good prediction of the downward liquid velocity with a constant value of the coefficient equal to 3 as well as with a value of the coefficient corresponding to the Deutsch relation. This is consistent as there is a strong relation between aeration of the airlift in the riser and in the downcomer and the resulting liquid circulation, induced by this difference of weight of column between the riser and the downcomer. The underestimation of the aeration of the downcomer observed for $C = 1$ corresponds to an underestimation of the liquid velocity.

The new data acquired in the frame of this study allow a more detailed analysis of each one of these simulations. Figures 7 and 8 show the horizontal profiles of void fraction

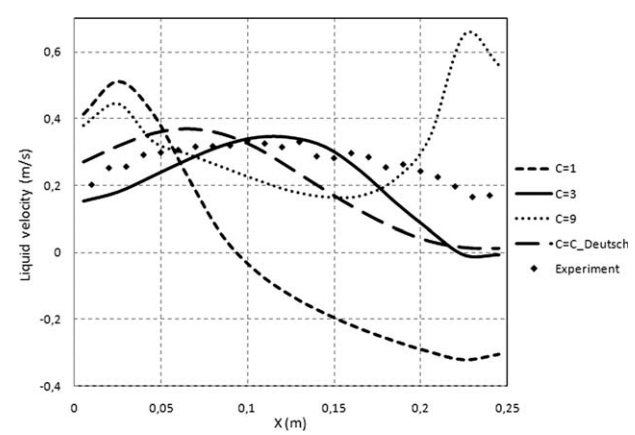

Figure 8. Horizontal profile of mean liquid velocity: experiments (full diamonds) compared with simulations.

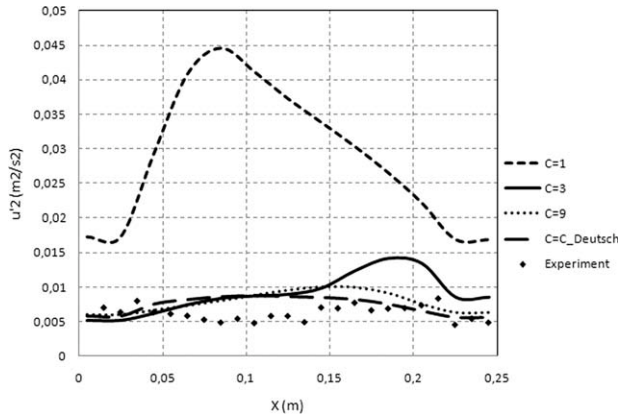

Figure 9. Horizontal profile of r.m.s. liquid velocity: experiments (full diamonds) compared with simulations.

and liquid velocity produced by the model in the riser, at a height of 2 m, for the four expressions of coefficient C.

Simulations Performed with C = *1.* In Figure 7, the simulated void fraction profiles are compared with the experimental data obtained at this section. Without turbulent contribution due to the added mass force ($C = 1$), the void fraction profile shows that the bubbles go toward the region where the turbulence is high, e.g., the pressure is low, close to the internal wall of the airlift reactor. In fact, Eq. 24 indicates that the pressure and the turbulence vary in opposite directions. Referring to Eq. 29 and considering $C = 1$, the y component of the relative velocity can be expressed as:

$$v_{Ry} = \tau_b \frac{\partial}{\partial y}\left[(1-\alpha)\overline{\overline{v'^2}}\right] = -\frac{\tau_b}{\rho}\frac{\partial \overline{\overline{p}}}{\partial y} \tag{38}$$

Clearly, when solely drag is considered, the momentum balance (38) indicates that the sign of the y component of the relative velocity of the bubbles, v_{R_y}, is opposite to the sign of the pressure gradient $\frac{\partial \overline{\overline{p}}}{\partial y}$ it means that the bubbles move toward low pressure regions ($v_{R_y} > 0$ as long as $\frac{\partial \overline{\overline{p}}}{\partial y} \leq 0$), which correspond also to high level of turbulence ($\frac{\partial \overline{\overline{v'^2}}}{\partial y} > 0$). The bubble migration toward the low pressure region produces a void fraction peaking. This trend is probably accentuated by the fact that the simulation is performed in 2-D. The buoyant effect due to the large void fraction in this region induces a significant acceleration of the liquid (Figure 8) and generates a significant shear stress. As a consequence, the turbulence production is enhanced and the simulation produces an increase of turbulent kinetic energy (Figure 9).

One can observe, in Figures 8 and 10, that the simulation corresponding to $C = 1$ is unable to reproduce the liquid and gas velocity profiles. Without physical modeling of dispersion, the simulated gas plume remains a nondispersive jet. The void fraction peaking produced by the simulation ($C = 1$) is not observed in the experiments nor the buoyant effect that accelerates the liquid in the high void fraction zone. Note also that the turbulence level produced in the shear zone is overestimated in comparison with the experimental data.

Simulations Performed with C = *3 and* C = $C_{Deutsch}$. - When the turbulent term due to the added mass force is introduced, the bubble migration toward the low pressure region is counterbalanced and the void fraction profile is significantly modified. In simulations SIM2 and SIM3, the peak of void fraction predicted by $C = 1$ is attenuated and moves toward the center of the riser. Thus, accounting for gas dispersion, both the void fraction profile (Figure 7) and the gas and liquid velocity profiles (Figures 8 and 9) are more homogeneous and satisfactorily close to the experiments.

Referring to Eq. 30 and considering $C = 3$, the y component of the relative velocity can be expressed as:

$$v_{Ry} = -\tau_b\left(1 + C_A\frac{C-1}{\alpha}\right)\overline{\overline{v'^2}}\frac{\partial \alpha}{\partial y} \approx -\frac{2}{3}\frac{\tau_b}{\alpha}k\frac{\partial \alpha}{\partial y} \tag{39}$$

In the case of a vertical gas plume, this term clearly shows that when the gas fraction decreases in the horizontal direction ($\frac{\partial \alpha}{\partial y} < 0$), for instance from the inside to the outside of the plume, it corresponds to a positive value of the y component of the relative velocity, resulting in a horizontal expansion of the gas plume. One can thus clearly explain the dispersion induced by this term. Consequently, the dispersion of the gas is larger for $C = 3$ than for $C = 1$ and is closer to the experiments.

SIM3. The expression of Deutsch coefficient has been given in Eq. 30. Recall that in air-water flow, the value of the parameter b is $b = 3$. In a previous work, Talvy et al.[38] have determined the expression of the ratio as follows:

$$\eta_r = \frac{1}{4}\frac{\Lambda}{r_b}\frac{1}{C_A} \tag{40}$$

where r_b is the bubble diameter and Λ is the turbulent Taylor macroscale. It can be scaled as:

$$\Lambda = \frac{\kappa}{C_\mu^{3/4}}y \approx 2.5\ y \tag{41}$$

where y is the distance to the wall. Given a bubble radius equal to 1.5 mm, when the distance to the wall varies between 3, 6, 9, 12, and 15 mm, the ratio η_r varies between 1, 2, 3, 4, and 5, and the Deutsch coefficient decreases between 5, 4, 3, 2.6, and

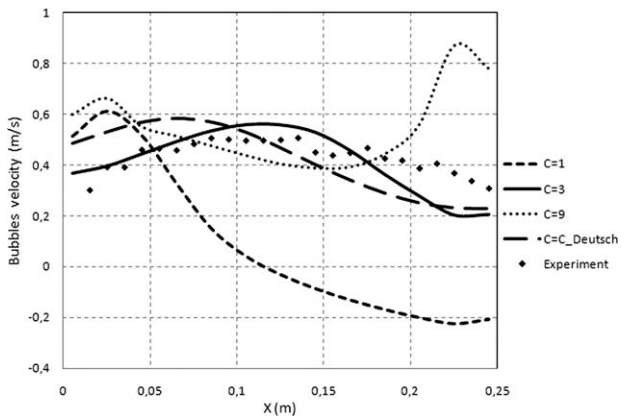

Figure 10. Horizontal profile of mean gas velocity: experiments (full diamonds) compared with simulations.

2.3. Consequently, it is obvious that a constant value of $C = 3$ corresponds fairly to the order of magnitude of the Deutsch coefficient.

Simulations Performed with C = 9. For the highest value of C coefficient ($C = 9$), the void fraction profile is completely inverted: just like in microgravity, the bubbles seem to escape the low pressure region (where the turbulence is high). Two symmetric void fraction peaks appear close to the walls. As a consequence, a non physical acceleration of the liquid (and the gas) velocity is simulated close to the wall of the airlift reactor. Clearly, overestimating C leads to unphysical void fraction peaks controlled by an overestimation of the role of turbulent kinetic energy gradient on the transverse migration of the bubbles.

The sensitivity analysis of the turbulent term due to the added mass force significantly modifies the void fraction profiles predicted by the numerical simulations, as compared to the experimental data (Figure 7). As a consequence, the effect of buoyancy is more homogenous and the average velocity profiles are strongly reorganized (Figures 8 and 10); the profiles of the turbulent energy follow this trend (Figure 9): as the shear is reduced, the turbulence production is decreased and the level of the turbulence is reduced. The simulations with the coefficient value $C = 3$ give good prediction in comparison with the experimental as well as predictions using C_{Deutsch} coefficient. One can observe (Figure 11) that the value of the coefficient C_{Deutsch} is close to 3, except close to the walls, where it is slightly larger. It should be observed that when the void fraction prediction is improved, the whole hydrodynamic of the internal loop gas-liquid airlift reactor is better predicted. Recall that, when the value of the coefficient C is close to 3, the effect of the turbulence on the bubbles distribution is inverted and the numerical results confirm this outcome. Accordingly depending on whether C is greater or lower than 3, the effect of the first term of the r.h.s. of Eq. 29 is inverted.

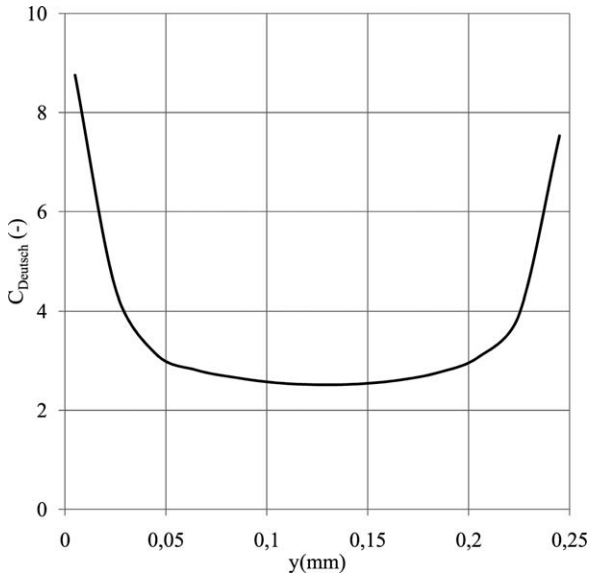

Figure 11. Horizontal profile of Deutsch coefficient derived from the simulation.

Discussion

In the discussion, it is interesting to compare this model to previous attempts of modeling of gas dispersion. Two works have been retained in this discussion, the model of Lopez de Bertodano and the model of Simonin.

Consider one more time the simplified case of quasi-parallel 2-D flow. The term including momentum transfer in the model of Chahed et al.[26] can be expressed as:

$$M_{\text{Gy}} = -\rho\frac{v_{\text{Ry}}}{\tau_{\text{b}}} - \frac{C_{\text{A}}}{\partial}\rho\frac{\partial}{\partial y}\left[\alpha(C-1)\overline{\overline{v'^2}}\right]$$

Considering the coefficient C to be constant and assuming isotropic turbulence, one can write:

$$M_{\text{Gy}} = -\rho\frac{v_{\text{Ry}}}{\tau_{\text{b}}} - \frac{2}{3}\frac{C_{\text{A}}}{\alpha}(C-1)\rho\frac{\partial}{\partial y}[\alpha\, k] \tag{42}$$

Clearly, this model accounts for both the gradient of gas fraction and the gradient of turbulent kinetic energy. Given a value of $C = 3$ which was shown to give good results and given a value of the added mass coefficient equal to 0.5, the previous relation becomes:

$$M_{\text{Gy}} = -\rho\frac{v_{\text{Ry}}}{\tau_{\text{b}}} - \frac{2}{3}\frac{1}{\alpha}\rho\frac{\partial}{\partial y}[\alpha\, k] = -\rho\frac{v_{\text{Ry}}}{\tau_{\text{b}}} - \frac{2}{3}\rho\frac{k}{\alpha}\frac{\partial\,\alpha}{\partial y} - \frac{2}{3}\rho\frac{\partial\, k}{\partial y} \tag{43}$$

where the two last term of r.h.s. of Eq. 43 come from the turbulent contribution of the added mass:

$$M_{\text{Gy}}^{\text{TAM}} = -\frac{2}{3}\frac{1}{\alpha}\rho\frac{\partial}{\partial y}[\alpha\, k] = \frac{2}{3}\rho\frac{k}{\alpha}\frac{\partial\alpha}{\partial y}\frac{2}{3}\rho\frac{\partial k}{\partial y} \tag{44}$$

This expression takes into accounts the gradient of gas fraction and the gradient of turbulent kinetic energy. In their model, Bel F'dhila and Simonin[23] introduced both the turbulent contribution of the added mass and the concept of drift velocity in the definition of drag. The term including momentum transfer in the model of Bel F'dhila and Simonin[23] can be expressed as:

$$M_{\text{Gy}} = -\rho\frac{v_{\text{Ry}} - v_{\text{drift},y}}{\tau_{\text{b}}} - \frac{C_{\text{A}}}{\alpha}\rho\frac{\partial}{\partial y}\left[\left(\frac{2}{3}q_{\text{G}} - \frac{1}{3}q_{\text{LG}}\right)\alpha\right] \tag{45}$$

q_{G} denotes the turbulent kinetic energy of the gas phase and q_{LG} denotes the co-variance between fluctuating velocities of the continuous flow and gas bubbles. Following Simonin and Viollet,[65] one can introduce the expression of the kinetic energy of the gas phase

$$q_{\text{G}}^2 = \frac{b^2 + \eta_{\text{r}}}{1 + \eta_{\text{r}}}k \tag{46}$$

The co-variance between fluctuating velocities of the continuous flow and gas bubbles is written as

$$q_{\text{LG}} = 2\frac{b + \eta_{\text{r}}}{1 + \eta_{\text{r}}}k \tag{47}$$

where b and η_r are, respectively, given by Eqs. 31 and 32. The added mass term proposed by Simonin can be simplified as follows:

$$M_{Gy}^{TAM} = -\frac{2}{3}\frac{C_A}{\alpha}\rho\frac{\partial}{\partial y}\left[\frac{b(b-1)}{1+\eta_r}\alpha\, k\right] \tag{48}$$

If this term is developed, assuming the ratio η_r is nearly constant, one obtains:

$$M_{Gy}^{TAM} \approx \frac{C_A b(b-1)}{1+\eta_r}\left[-\frac{2}{3}\rho\ \ \frac{\partial k}{\partial y} - \frac{2}{3}\rho\frac{k}{\alpha}\frac{\partial \alpha}{\partial y}\right] \tag{49}$$

Comparing Eq. 49 with Eq. 44, these expressions are proportional. Following Talvy et al.[38] the coefficient $\frac{C_A b(b-1)}{1+\eta_r}$ can be estimated; when η_r varies between 1 and 5, this coefficient varies between 3/2 and 1/2. As far as different parameters are assumed to be constant (the coefficient C and the ratio η_r) and despite the difference in their analytical derivations, the orders of magnitudes of the turbulent contributions of the added mass term proposed by Chahed et al.[26] (Eq. 44) and Bel F'dhila and Simonin[23] (Eq. 49) are close to each other.

In addition, it is interesting to focus on the drift velocity term introduced by Bel F'dhila and Simonin[23] in Eq. 45:

$$M_{Gy}^{drift} = \rho\frac{v_{drift,y}}{\tau_b} = \rho\frac{1}{\tau_b}D_{GL}^t\frac{1}{\alpha(1-\alpha)}\frac{\partial \alpha}{\partial y} \tag{50}$$

where the turbulent dispersion is given by

$$D_{GL}^t = \frac{1}{3}q_{GL}\tau_{GL}^t \tag{51}$$

In Talvy et al.,[36] it was shown that the dispersion coefficient D_{GL}^t in air-water bubbly flow can be simplified as:

$$D_{GL}^t = \frac{1}{3}q_{GL}\tau_{GL}^t \approx C' C_\mu \frac{k^2}{\varepsilon} \tag{52}$$

Hence, the drift term becomes:

$$M_{Gy}^{drift} = \rho\frac{v_{drift,y}}{\tau_b} = \rho C' C_\mu \frac{k/\varepsilon}{\tau_b}\frac{k}{\alpha(1-\alpha)}\frac{\partial \alpha}{\partial y} \tag{53}$$

which is very similar to the turbulent dispersion term proposed by Lopez de Bertodano. Lopez de Bertodano[68] did not take into account the turbulent contribution of the added mass, but proposed a two-fluid model including an additional term of turbulent dispersion as follows:

$$M_{Gy}^{TD} = -\frac{C_{TD}}{\alpha}\rho\, k\frac{\partial \alpha}{\partial\, y} \tag{54}$$

The turbulent dispersion coefficient is expressed as:

$$C_{TD} = C_\mu^{1/4}\frac{1}{St(1+St)} \tag{55}$$

where the local Stokes number $St = \frac{\tau_b}{\tau_{LB}^t}$ is the ratio of a characteristic time scale of bubbles τ_b given by Eq. 18 and a characteristic time scale of the turbulence in the liquid τ_{LB}^t given by $\tau_{LB}^t = C_\mu^{3/4}\frac{k}{\varepsilon}$. Thus, one can derive:

$$M_{Gy}^{TD} = -\rho\frac{1}{1+St}\frac{k/\varepsilon}{\tau_b}\frac{k}{\alpha}\frac{\partial \alpha}{\partial y} \tag{56}$$

The expressions (56) from turbulent dispersion term proposed by Lopez de Bertodano and (53) from drift velocity term introduced by Simonin are also similar. It should be recalled that none of these terms have been introduced in the present modeling.

The model of Chahed et al.[18] tested here includes both the effects of gradient of gas fraction and of gradient of turbulent kinetic energy, without introducing an additional turbulent dispersion term and without introducing a drift velocity. The main difference between the turbulent contribution of added mass derived by Chahed et al.[18] tested in this article, and by Bel F'dhila and Simonin[23] comes from the definition of material derivatives. Bel F'dhila and Simonin[23] derived the expression of the instantaneous added mass force, assuming that the material derivatives associated to the phase gas $\frac{d..}{dt}$ and to the liquid phase $\frac{D..}{Dt}$ were identical. Chahed et al.[18] derived the formulation of the added mass taking into account the difference between both types of material derivatives, obtaining the general expression of the average and fluctuating contributions of the mass added term which has been used in this work. One of the main conclusions of Talvy et al.[38] was that closure accounting for the turbulent contributions via the drift velocity improved the prediction of the flow in the air-lift reactor. This work confirms that it is essential to account for gas dispersion but it shows that this can be done by simply accounting for the turbulent contribution of the added mass term.

To clarify the specific effects of the two turbulent contributions of the added mass force, a last series of simulations was performed, in which only the effect of dispersion proportional to the gradient of void fraction was taken into account. In this case, the y component of the momentum transfer (Eq. 42) is written as:

$$M_{Gy} = -\rho\frac{v_{Ry}}{\tau_b} - \frac{2}{3}\frac{C_A}{\alpha}(C-1)\rho\, k\frac{\partial \alpha}{\partial y}$$

The numerical simulations are performed with values of C ranging from 1 to 9, and we adopt the same conditions as in the first series of simulations. Recall that the simulation with the coefficient ($C = 1$) leads to a particular situation where no turbulent contribution to the added mass has been considered. One finds in this case the pressure effect that produces, as in previous simulations, a peak of void fraction in the region of high turbulence, Figure 12.

The simulations performed with $C > 1$ reveal a bubble dispersion that leads to the flattening of the void fraction profile. When the coefficient C increases, the effect of turbulent dispersion is enhanced. With the largest value ($C = 9$), the void fraction profile becomes almost completely flat, but without inversion and without void fraction peak close to the walls, as it occurs in the previous simulations carried out with the two turbulent contributions of the added mass force.

Overall, the results produced by these last series of simulations are less accurate than the results produced by the previous simulations that take into account the two contributions of the added mass force, although in both cases, the turbulent dispersion improves the results compared with the

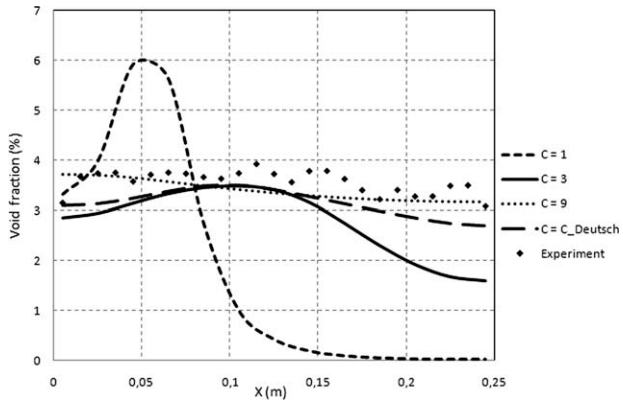

Figure 12. Horizontal profile of void fraction: experiments (full diamonds) compared with simulations.

case with $C = 1$. However, it seems that the new term due to the added mass, which is proportional to the gradient of the turbulent energy, improves the prediction of the radial distribution of the void fraction, although its effect appears weaker than in the simulation of pipe bubbly flow in micro-gravity conditions. In fact, it should be observed that in the core of the airlift reactor, the flow is almost homogeneous and the turbulence gradient is weak compared with the case of bubbly flow in micro-gravity condition where the wall turbulence produces high turbulence gradient. In micro gravity, this term has a more important role since it represents the only driving force that explains the inversion of the void fraction gradient producing the void fraction maximum observed in the centreline of the pipe.

Conclusions

Gas–liquid reactors are multiphase devises where the interfacial interactions and exchanges are often the technological reason for the process. Local multiphase analysis constitutes a decisive progress in the claboration of suitable computational fluid dynamics tools for gas-liquid systems. One of the main issues of the two- phase flow modeling is to achieve a sufficiently accurate prediction of local characteristics of the flow (average velocities, turbulent intensity, and phase distribution) especially in buoyancy driven bubbly flows such as air-lifts and bubble columns. In these particular gas-liquid systems, the gas distribution represents the only forcing that determines the hydrodynamics in the reactor.

The numerical and experimental analysis of the gas-liquid flow in the airlift presented in this article aim to precise the role played by the turbulence in the interfacial momentum transfer. Gas dispersion in air-lift reactors is evaluated on the basis of numerical simulations using an Eulerian two-fluid model and the numerical results are compared to local experimental data. The effect of the interfacial momentum transfer modeling in the phase distribution phenomenon is discussed and the analysis is focused on the role played by the turbulent contributions. For this purpose, different numerical simulations are performed with various interfacial momentum transfer models and the void fraction distribution is analysed with respect to the effect of the turbulent terms in the interfacial momentum transfer.

The turbulence has two main effects on the gas distribution through the gas-liquid reactor: First, the turbulence of the liquid phase induces a pressure effect that directly acts on the bubbles displacements. Second, the interfacial momentum exchange includes beside the average contribution (the average force) a turbulent contribution issued from the averaging of the force exerted by the liquid on the bubbles. The common method consists in considering only the mean contributions of the force when the turbulent contributions are ignored or represented by a global dispersion effect.

This work confirms that closure accounting for the turbulent contributions via the drift velocity improves the prediction of the flow in the air-lift reactor but it shows that this can be done by simply accounting for the turbulent contribution of the added mass term. Indeed, the turbulent term coming from the averaging of the added mass force may be split into two turbulent terms: the first one is proportional to the void fraction gradient and consequently has a similar effect than the drift velocity; the second turbulent term is proportional to the gradient of the turbulent energy and its effect is comparable with the effect of the pressure gradient. This term contains turbulent correlations of the liquid and of the gas. We have to provide accurate closures not only for the turbulence in the liquid but also for the turbulence in the gas. The objective of the present study is to analyze the sensitivity of the model to the turbulent contribution of the added mass force and thus a crude model for the turbulence of the gas phase has been used. In this model, the turbulent correlations of the gas are related to that of the liquid using an adjustable coefficient. A constant value of this coefficient fixed to unity suppresses the effect of the turbulent contribution of the added mass force and strongly underestimates the gas dispersion. A constant value fixed to 9 overestimates the gas dispersion. Indeed, the value of the coefficient fixed to 3 gives good results, in accordance with the results obtained using Deutsch model. Therefore, from these simulations it is clear that the expression proposed by Deutsch and derived from Tchen theory is a good candidate to relate the turbulent stress in the gas to the turbulent stress tensor in the liquid.

The results produced by the simulations that take into account the two turbulent contributions of the added mass force improve the prediction of the transverse distribution of the void fraction. These numerical simulations and the analysis of the transverse displacements of the bubbles in the air lift provide evidence that the turbulence plays an important part on the bubbles distribution not only by the pressure term, but also by the turbulent contribution of the interfacial force. Therefore, it is crucial to take into account the contribution of the turbulence in the interfacial momentum transfer, particularly in the added mass term. These simulations show that the turbulent contributions of the added mass force play an important role in the phase distribution phenomenon and confirm previous results obtained in studying gas-liquid bubbly flows under micro-gravity conditions. However, further theoretical and numerical developments as well as new specific experiments are needed to explore the role of the other turbulent contributions in the interfacial momentum balance.

Acknowledgments

Support of this research by CMCU project 04PRE01 and Institut Francais de Coopération (IFC) at Tunis is gratefully acknowledged. The authors thank Véronique Roig (IMFT, Toulouse, France) for her support on data acquisition and processing.

Notation

b = coefficient
C = coefficient
C_A = added mass coefficient
C_D = drag coefficient
C_{TD} = turbulent dispersion coefficient
$C_{Tchen\text{-}Hinze}$ = Tchen-Hinze coefficient
$C_{Deutsch}$ = Deutsch coefficient
C_β = crossing trajectory coefficient
C_μ = turbulent viscosity constant
d_b = bubble diameter, m
D_{GL}^t = fluid-bubble turbulent dispersion, $m^2\ s^{-1}$
$E\ddot{o}$ = Eötvos number
g = gravity acceleration, $m\ s^{-2}$
j_k = superficial phase velocity, $m\ s^{-1}$
k = turbulent kinetic energy (TKE), $m^{-2}\ s^{-2}$
k_s = pseudo-turbulent kinetic energy (TKE), $m^{-2}\ s^{-2}$
M_G = local instantaneous interfacial momentum transfer, $kg/m^{-2}\ s^{-2}$
M_{Gy}^D = interfacial momentum transfer associated to drag, $kg\ m^{-2}\ s^{-2}$
M_G^{AM} = interfacial momentum transfer associated to added mass, $kg\ m^{-2}\ s^{-2}$
M_G^{TAM} = momentum transfer associated to turbulent contribution of added mass, $kg\ m^{-2}\ s^{-2}$
M_G^{drift} = momentum transfer associated to drift velocity, $kg\ m^{-2}\ s^{-2}$
M_G^{TD} = interfacial momentum transfer associated to turbulent dispersion, $kg\ m^{-2}\ s^{-2}$
p = pressure, $kg\ m^{-1}\ s^{-2}$
q_G = turbulent kinetic energy in the gas phase, $m^{-2}\ s^{-2}$
q_{LG} = co-variance between fluctuating velocities of liquid and bubbles, $m^{-2}\ s^{-2}$
Re = Reynolds number
r_b = bubble radius, m
St = Stokes number
t = time, s
u = local instantaneous liquid velocity, $m\ s^{-1}$
u_G = local instantaneous gas velocity, $m\ s^{-1}$
u_k' = local instantaneous turbulent component of phase velocity, $m\ s^{-1}$
$\overline{u_{Gi}'u_{Gj}'}$ = gas phase Reynolds stress tensor, $m^2\ s^{-2}$
$\overline{u_i'u_j'}$ = liquid phase Reynolds stress tensor, $m^2\ s^{-2}$
u_R = relative velocity, $m\ s^{-1}$
v_{drift} = drift velocity, $m\ s^{-1}$
x = vertical coordinate, m
y = horizontal coordinate, m

Greek letters

α = gas fraction
κ = von Karman constant
δ_{ij} = Kronecker symbol
ε = dissipation rate of the TKE, $m^2\ s^{-3}$
Φ = instantaneous variable
Λ = Taylor macroscale of the turbulence in the liquid phase, m
ρ = liquid density, $kg\ m^{-3}$
ρ_G = gas density, $kg\ m^{-3}$
τ = characteristic time scale, s
τ_b = bubble characteristic time scale, s
τ_{GL}^t = characteristic time scale of the turbulence seen by the gas phase, s
τ_{GL}^F = characteristic time scale of bubble entrainment by liquid motion, s
τ_I^t = turbulent characteristic time scale, s
V_t = turbulent viscosity, $m^2\ s^{-1}$
ζ_r = ratio of the characteristic time of the turbulence in the liquid and the characteristic time scale of the bubble necessary to cross the containing energy eddies
η_r = ratio of the characteristic time scale of the turbulence seen by the gas phase, denoted τ_{GL}^t and the characteristic time scale of the bubble entrainment by the liquid motion τ_{GL}^F
σ = surface tension, $kg\ s^{-2}$

Literature Cited

1. Lance M, Bataille J. Turbulence in the liquid phase of a uniform bubbly air water flow. *J Fluid Mech*. 1991;222:95–118.
2. Roig V, Suzanne C, Masbernat L. Experimental investigation of a turbulent bubbly mixing layer. *Int J Multiphase Flow*. 1998;24:35–54.
3. Lance M, Marié JL, Bataille J. Homogeneous turbulence in bubbly flows. *J Fluids Eng*. 1991;113:295–300.
4. Serizawa A, Kataoka I. Turbulence suppression in bubbly two-phase flow. *Nucl Eng Des*. 1990;122:1–16.
5. Chahed J. Forces interfaciales et turbulence dans les écoulements à bulles: Modélisation et étude de cas de référence. Thèse de Doctorat ès Sciences de l'Ecole Nationale d'Ingénieurs de Tunis, 1999.
6. Troshko AA, Hassan YA. A two-equation turbulence model of turbulent bubbly flows. *Int J Multiphase Flow*. 2001;27:1965–2000.
7. Wang SK, Lahey RT, Jones OC. Three dimensional turbulence structure and phase distribution measurements in bubbly two phase flows. *Int J Multiphase Flow*. 1987;13:327–343.
8. Serizawa A, Kataoka I, Michiyoshi I. *Phase distribution in bubbly flow* In: Hewit GF, Delahay JM, Zuber N, editors. *Multiphase Science and Technology*, Vol. 6. Hemisphere Publishing Corporation, 1992:257–301.
9. Mareuge I, Lance M. *Bubble-induced dispersion of a passive scalar in bubbly flows*. In: *Proceeding of the 2nd International Conference on Multiphase Flow*, Kyoto, April 3–7, 1996.
10. Ellingsen K, Risso F. On the rise of an ellipsoidal bubble in water; oscillatory paths and liquid-induced velocity. *J Fluid Mech*. 2001;440:235–268.
11. Lee SJ, Lahey RT, Jones OC. The prediction of two phase turbulence and phase distribution phenomena using k,ε model. *Jpn J Multiphase Flow*. 1989;3:335–368.
12. Lopez de Bertonado M, Lee SJ, Lahey RT, Drew DA. The prediction of two-phase turbulence and phase distribution using a Reynolds stress model. *J Fluids Eng*. 1990;112:107–113.
13. Simonin O. *Second momentum prediction of dispersed phase turbulence in particle laden flows*. In: *Proceedings of 8th Symposium on Turbulent Shear Flows*, Munich, September 9–11, 1991.
14. Wang DM, Issa RI, Gosman AD. *Numerical prediction of dispersed bubbly flow in a sudden enlargement*. In: Crowe CT, et al., editors. *Numerical Methods in Multiphase Flows*. In: *Presented at the 1994 ΔSME Fluids Engineering Division Summer Meeting*, Lake Tahoe, NV, USA, June, 19–23, Vol. 185, ASME, New York, 1994:141–148.
15. Morel C. Modélisation multidimensionnellc des écoulements diphasiques gaz-liquide. Application à la simulation des écoulements à bulles ascendants en conduite verticale. Thèse de doctorat de l'Ecole Centrale de Paris, 1997.
16. Sato Y, Sadatomi L, Sekoguchi K. Momentum and heat transfer in two phase bubbly flow. *Int J Multiphase Flow*. 1981;7:167–190.
17. Lopez de Bertonado M, Lee SJ, Lahey RT, Jones OC. Development of a k-ε model for bubbly two-phase flow. *J Fluids Eng*. 1994;116:128–134.
18. Chahed J, Roig V, Mabernat L. Eulerian-Eulerian two-fluid model for turbulent bubbly flows. *Int J Multiphase Flow*. 2003;29:23–49.
19. Bellakhal G, Chahed J, Masbernat L. Analysis of the turbulence structure in homogeneous shear bubbly flow using a turbulent viscosity model. *J Turbul* 2004;5:036.
20. Drew DA, Lahey RT. Phase distribution mechanisms in turbulent low-quality two-phase flow in circular pipe. *J Fluid Mech*. 1982;117:91–106.
21. Kamp A, Colin C, Fabre J. Techniques de mesure par sonde optique double en écoulement diphasique a bulles. Colloque de Mécanique des Fluides Expérimentale, Cert Onera, Toulouse, France, 1995.

22. Bel F'Dhila R. Analyse expérimentale et modélisation d'un écoulement vertical à bulles dans un élargissement brusque. Thèse Spécialité: Mécanique des Fluides, Institut National Polytechnique de Toulouse, France, 1991.
23. Bel F'dhila R, Simonin O. Eulerian prediction of a turbulent bubbly flow downstream of a sudden pipe expansion. In: *6th Workshop on Two-Phase Flow Predictions*, Erlangen, 30 March-2 April, 1992.
24. Wang DM, Issa RI. Two phase turbulence modelling—a review. Technical report 11–14. BRITE/EURAM. Project BE 4098, September, 1992.
25. Lance M. Lopez de Bertonado M. Phase distribution phenomena and wall effects in bubbly two-phase flows. In: *3rd International Workshop on Two-Phase Flow Fundamentals, Imperial College*, London, June 15–19, 1992.
26. Chahed J, Colin C, Masbernat L. Turbulence and phase distribution in bubbly pipe flow under micro-gravity condition. *J Fluids Eng*. 2002;124:951–956.
27. Sokolichin A. Eigenberger G. Gas–liquid flow in bubble columns and loop reactors, part 1. Detailed modeling and numerical simulation. *Chem Eng Sci*. 1994;49:5735–5746.
28. Becker S. Sokolichin A, Eigenberger G. Gas–liquid flow in bubble column and loop reactors, part 2. Comparison of detailed experiments and flow simulation. *Chem Eng Sci*. 1994;49:5747–5762.
29. Celik I, Wang YZ. Numerical simulation of circulation in gas-liquid column reactors: isothermal, bubbly, laminar flow. *Int J Multiphase Flow*. 1994;20:1053–1070.
30. Grevskott, S, Sannaes BH, Dudukovic MP, Hjarbo KW, Svendsen HF. Liquid circulation, bubble size distribution and solids movement in two- and three-phase bubble columns. *Chem Eng Sci*. 1996;51:1703–1713
31. Chisti Y. *Airlift Bioreactors*. New York: Elsevier Applied Science, 1989.
32. Talvy S, Cockx A, Liné A. Global modelling of a gas-liquid-solid airlift reactor. *Chem Eng Sci* 2005;60:5991–6003.
33. Cockx A. Do-Quang Z, Liné A, Roustan M. Use of computational fluid dynamics for simulating hydrodynamics and mass transfer in industrial ozonation towers. *Chem Eng Sci*. 1999;54:5085–5090.
34. Cockx A. Liné A, Roustan M, Doquang Z, Lazarova V. Numerical simulation and physical modeling of the hydrodynamics in an air-lift internal loop reactor. *Chem Eng Sci*. 1997;52:3787–3793.
35. Mudde RF, van den Akker HEA. 2D and 3D simulations of an internal airlift loop reactor on the basis of a two- fluid model. *Chem Eng Sci*. 2001;56:6351–6358.
36. Van Baten JM, Ellenger J, Krishna R. Using CFD to describe the hydrodynamics of internal airlift reactors. *Can J Chem Eng*. 2003;81:660–668.
37. Oey RS, Mudde RF, van den Akker HEA. Numerical simulations of an oscillating internal-loop airlift reactor. *Can J Chem Eng*. 2003;81:684–691.
38. Talvy S, Cockx A, Liné A. Modeling hydrodynamics of gas-liquid airlift reactor. *AIChE J* 2007;53:335–353.
39. Talvy S, Cockx A, Liné A. Modeling of oxygen mass transfer in a gas-liquid airlift reactor. *AIChE J* 2007;53:316–326.
40. Sato Y, Sekoguchi K. Liquid velocity distribution in two-phase bubble flow. *Int J Multiphase Flow*. 1975;2:79–95.
41. Tchen C M. Mean in value and correlation problems connected with the motion of small particles suspended in a turbulent fluid. PhD Technische Hogeschool Delft, 1947.
42. Deutsch E. Dispersion des particules dans une turbulence homogène isotrope stationnaire calculée par simulation numérique directe des grandes échelles. Thèse de Doctorat INPT, Toulouse, France, 1992.
43. Csanady GT. Turbulent diffusion of heavy particles in the atmosphere. *J Atmos Sci*. 1963;20:201–208.
44. Bel F'dhila R, Duineveld PC. The effect of surfactant on the rise of spherical bubble at high Reynolds and Peclet numbers. *Phys Fluids*. 1996;8:310–321.
45. Clift R, Grace J R, Weber ME. *Bubbles, Drops and Particles*. Academic Press: New York, 1978.
46. Zuber N, Ishii M. Drag coefficient and relative velocity in bubbly, droplet or particulate flows. *AIChE J* 1979;25:843–855.
47. Leon Bécerril E, Liné A. Effect of bubble deformation on stability and mixing in bubble column. *Chem Eng Sci*. 2002;57:3283–3297.
48. Drew DA, Passman SL. *Theory of Multicomponent Fluids*. New York: Springer, 1999.
49. Lahey RT, Lopez de Bertodano M, Jones OC. Phase distribution in complex geometry ducts. *Nucl Eng Des*. 1993;141:177–201.
50. Carrica PM, Drew DA, Lahey RT. A polydisperse model for bubbly two-phase flow around a surface ship. *Int J Multiphase Flow*. 1999;25:257–305.
51. Drew DA. A turbulent dispersion model for particles and bubbles. *J Eng Math*. 2001;41:259–274.
52. Moraga FJ, Larreteguy AE, Drew DA, Lahey RT. Assessment of turbulent dispersion models for bubbly flows in the low Stokes number limit. *Int J Multiphase Flow*. 2003;29:655–673.
53. Legendre D. Quelques aspects des forces hydrodynamiques et des transferts de chaleur sur une bulle sphérique. Thèse de Doctorat de l'Institut National Polytechnique de Toulouse, France, 1996.
54. Legendre D, Magnaudet J. Interaction between two spherical bubbles rising side by side. In: *3th International Conference on Multiphase Flow*, Lyon, France, 1998.
55. Sokolichin A, Eigenberger G, Lapin A. Simulation of buoyancy driven bubbly flow: established simplifications and open questions. *AlChE J*. 2004;50:24–45.
56. Couvert A. Etude d'un réacteur airlift rectangulaire à recirculation interne. Thèse de doctorat de l'INSA de Toulouse, France, 2000.
57. Cockx A. Modélisation de contacteurs gaz-liquide: application de la mécanique des fluides numériques aux airlifts. Thèse de doctorat de l'INSA de Toulouse, France, 1997.
58. Farrar B. Bruun HH. Interaction effects between a cylindrical hot-film anemometer probe and bubbles in air/water and oil/water flows. *J Phys Instrum*. 1989;22:114–123.
59. Larue de Tournemine A. Etude expérimentale de l'effet du taux de vide en écoulements diphasiques à bulles. Thèse de doctorat de l'Institut National Polytechnique de Toulouse, France, 2001.
60. Roig V. Zones de melange d'écoulements diphasiques à bulles. Thèse de doctorat de l'Institut National Polytechnique de Toulouse, France, 1993.
61. Kamp A. Ecoulements turbulents à bulles dans une conduite en micropesanteur. Thèse de doctorat de l'Institut National Polytechnique de Toulouse, France, 1996.
62. Hébrard G. Influence du distributeur de gaz en colonne à bulles. Thèse de doctorat de l'INSA de Toulouse, France, Toulouse, 1995.
63. Bellakhel G. Influence du distributeur de gaz en colonne à bulles. Thèse de Doctorat de l'Institut National Polytechnique de Toulouse, France et de l'Ecole Nationale d'Ingénieurs de Tunis, Tunisie, 2005.
64. Ayed H, Chahed J, Roig V. Experimental analysis and numerical simulation of hydrodynamics and mass transfer in a turbulent buoyant shear layer. *AlChE J* 2007;53:2742–2753.
65. Simonin O, Viollet PL. *Modelling of turbulent two-phase jets loaded with discrete particles*. In: Hewitt G, Mayinger F, Riznie JR, editors. *Phase Interface Phenomena in Multiphase Flow*. Hemisphere Publishing Corporation, 1990; 259–270.
66. Simonin O, Viollet PL. Prediction of an oxygen droplets pulverization in a compressible subsonic coflowing hydrogen flow. In: *Symposium on Numerical Methods for Multiphase Flows*, Toronto, Canada, June 4–7, 1990.
67. Simonin O. *Eulerian formulation for particle dispersion in turbulent two-phase flows*. In: *Proceedings of 5th Workshop on Two- Phase Flow Predictions*, Erlangen, FRG, March 19–22, 1990.
68. Lopez de Bertodano M. Two fluid model for two-phase turbulent jets. *Nucl Eng Des* 1998;179:65–74.
69. Merchuk JC. Airlift bioreactors: review of recent advances. *Can J Chem Eng*. 2003;81:324–337.

Manuscript received July 3, 2010, revision received Oct. 27, 2010, and final revision received Dec. 21, 2010.